EVIDENCE OF A CURVED COSMIC-RAY ELECTRON SPECTRUM IN THE SUPERNOVA REMNANT SN1006

G. E. Allen
MIT Center for Space Research
77 Massachusetts Avenue, NE80-6029, Cambridge, MA 02139-4307, USA
GEA@SPACE.MIT.EDU
J. C. Houck, S. J. Sturner
HOUCK@SPACE.MIT.EDU, STURNER@SWATI.GSFC.NASA.GOV

Abstract

A joint spectral analysis of some *Chandra* ACIS data, some radio data and the CANGAROO γ-ray data was performed for the eastern rim of the supernova remnant SN1006. These data were fitted with a model that includes synchrotron radiation and inverse-Compton scattering of the cosmic microwave background. The non-thermal electron spectrum used to compute the emission spectra for these two components is the traditional exponentially cut-off power law with one notable difference. The power-law index is not a constant. It is a logarithmic function of the momentum. This functional form enables us to show, for the first time, that the electron spectrum of SN1006 seems to flatten with increasing energy. At 1 GeV (i.e., radio–synchrotron-emitting energies), the power-law index is about 2.2. At 30 TeV (i.e., X-ray–synchrotron-emitting energies), the index is about 2.0. This result is quantitatively consistent with theoretical models of the amount of curvature in the proton spectrum of SN1006 and implies that cosmic rays are dynamically important, not "test" particles.

1 Introduction

Several observational and theoretical clues support the suggestion that Galactic cosmic rays, up to an energy of at least 100 TeV (Lagage & Cesarsky, 1983), are accelerated predominantly in the shocks of supernova remnants. In this case, an average supernova remnant must transfer about 10% of its kinetic energy to cosmic rays, which means that the cosmic-ray energy density or pressure at the shock is significant and may affect the shock structure.

One potentially observable consequence of a large cosmic-ray pressure is that the shock transition region is broadened or "smeared out," not abrupt. In this case, low-energy cosmic rays, which have relatively small diffusion lengths, experience only a portion of the velocity gradient as they scatter back and forth across the shock. Higher-energy particles, which have relatively large diffusion lengths, experience a larger portion (or all) of the velocity jump. Since the rate of energy gain increases as the velocity difference increases, higher-energy particles gain energy faster than lower-energy particles. As a result, cosmic-ray spectra do not have power-law distributions. The spectra flatten with increasing energy (Ellison, Berezhko & Baring, 2000). Jones et al. (2003) demonstrate that the radio-to-infrared spectra of small, selected regions of the Cas A remnant flatten with increasing energy. This evidence shows that the cosmic-ray electrons producing the synchrotron emission have a curved spectrum. Evidently, the cosmic-ray ions and electrons in Cas A have modified the structure of the shock.

2 Data and analysis

This paper describes the results of joint spectral analysis of some X-ray, radio and γ-ray data for the remnant SN1006. X-ray spectra of the filaments along the eastern rim of the remnant were obtained by analyzing 68 ks of data from the 2000 July 10–11 *Chandra* observation of the source. The X rays were detected using the Advanced CCD Imaging Spectrometer (ACIS). Each 1024×1024 pixel CCD has a field of view of $8\farcm4\times8\farcm4$. The on-axis effective area for the mirrors and ACIS-S3 has a maximum of about 720 cm^2 at 1.5 keV and is greater than 10% of this value for energies between

about 0.3 and 7.3 keV. The fractional energy resolution (FWHM/E) between these energies ranges from about 0.4 to 0.03, respectively. The sensitive energy bands and energy resolutions of the other five CCDs used for SN1006 are typically worse than the energy band and resolution of ACIS-S3.

The ACIS data were filtered to remove the events that (1) have GRADE = 1, 5, or 7, (2) have one or more of the STATUS bits set to one (except for events that only have one or more of the four cosmic-ray "afterglow" bits set), (3) are part of a horizontal "streak" on ACIS-S4 or (4) occur in the time interval during which the mean background count rate was more than twice the nominal rate (i.e., frames 20515–21294). An image of the 66 ks of "good" data is displayed in Fig. 1. The thirteen 100×100 pixel ($\approx 49'' \times 49''$) boxes along the bright filaments of the eastern rim of Fig. 1 are the regions used for spectral analysis. The PHA spectra, ARFs and RMFs for each region were created using standard `CIAO` tools. The ARFs were adjusted for the effects of a build up of absorbing material on the instruments. The X-ray analysis was performed using data in the energy band 2–7 keV.

The radio spectral data used for the spectral analysis include the compilation described by Allen, Petre & Gotthelf (2001) and includes the 843 MHz observation by Roger et al. (1988). The radio spectra for regions 1–13 were constructed by multiplying the flux densities and uncertainties by the factors f listed in Table 1. For each of the thirteen regions, the factor f was computed by dividing the 843 MHz flux density for that region by the total 843 MHz flux for the entire remnant. Since the radio spectrum for the entire remnant is used to construct radio spectra for each region, we are assuming that the shape of the radio spectrum for each region is the same as the shape of the radio spectrum of the entire remnant.

The γ-ray spectrum used for the spectral analysis is the spectrum presented by Tanimori et al. (2001). Since we have no information about the fraction of the γ-ray emission produced in each of the thirteen regions, the same γ-ray spectrum is used for each region.

The spectral data for each region were fitted in ISIS (Houck & Denicola, 2000) with a model that includes interstellar absorption for the X-ray data, synchrotron radiation for the X-ray and radio data and inverse-Compton scattering of the cosmic microwave background for the γ-ray data. Since the 2–7 keV emission

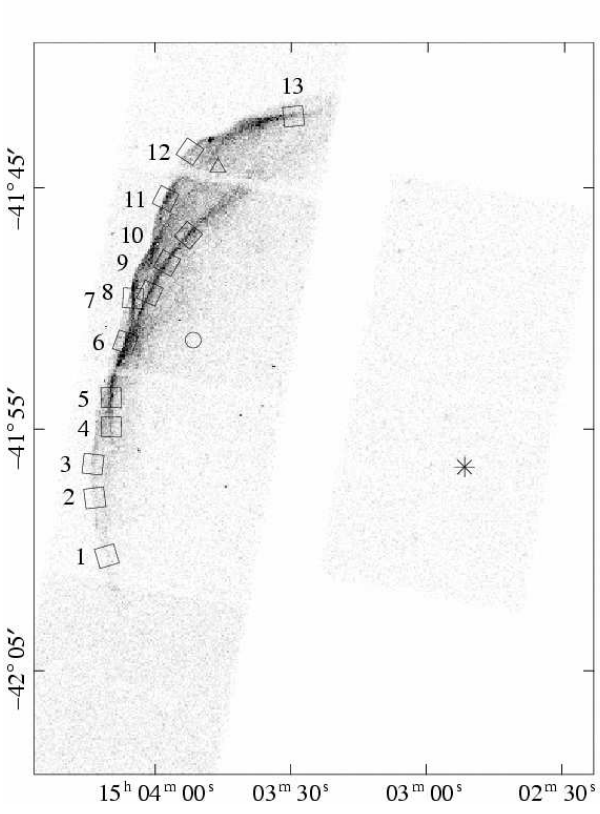

Figure 1: A 2–7 keV ACIS image of the eastern rim of SN1006. The regions labeled 1–13 are the regions used to perform spectral analysis. The circle, asterisk and triangle indicate the locations of the nominal aim point of the telescope, the center of the supernova remnant (Winkler & Long, 1997) and the centroid of the TeV source (Tanimori et al., 1998), respectively.

is dominated by non-thermal emission, no thermal X-ray component is included.

The synchrotron and inverse-Compton emission spectra are based on an electron spectrum of the form

$$\frac{dn}{dpc} = A \left(\frac{pc}{\mathrm{GeV}} \right)^{-\Gamma + a \log\left(\frac{pc}{\mathrm{GeV}}\right)} e^{\left(\frac{\mathrm{GeV}-E}{\epsilon}\right)}, \qquad (1)$$

where n is the electron number density, $p = \gamma m v$, v is the velocity of a particle, c is the speed of light, A is the number density at p = 1 GeV/c (in units of cm^{-3} GeV^{-1}), Γ is the differential spectral index at p = 1 GeV/c, a is the spectral "curvature," the logarithm is base ten, $E = \gamma m c^2$, and ϵ is the exponential cut-off (or "maximum") energy. This form is the same as the standard power law with an exponential cut off, except for the term $a \log (pc/\mathrm{GeV})$. Introduction of this term produces an effective spectral index, $\Gamma - a \log (pc/\mathrm{GeV})$, that is a linear function of the log-

Table 1: Best-fit parameters

Region	RA (h m s)	Dec. (° ′ ″)	f	Γ	a	ϵ (TeV)	B (μG)	ν_c (10^{16} Hz)	χ^2/dof
1	15 04 10.7	−42 00 15	0.0010	$2.24^{+0.13}_{-0.13}$	$0.051^{+0.058}_{-0.043}$	25^{+29}_{-11}	$2.5^{+8.5}_{-1.7}$	$2.1^{+6.9}_{-1.4}$	9.9/22
2	15 04 13.3	−41 57 51	0.00089	$2.27^{+0.08}_{-0.11}$	$0.073^{+0.042}_{-0.038}$	22^{+19}_{-9}	$2.8^{+6.2}_{-1.8}$	$1.9^{+2.5}_{-0.9}$	14.1/26
3	15 04 13.7	−41 56 27	0.00069	$2.27^{+0.13}_{-0.12}$	$0.079^{+0.039}_{-0.029}$	21^{+17}_{-8}	$3.7^{+7.0}_{-2.3}$	$2.3^{+2.2}_{-1.0}$	11.6/31
4	15 04 09.7	−41 54 54	0.0024	$2.22^{+0.14}_{-0.11}$	$0.050^{+0.034}_{-0.027}$	22^{+17}_{-7}	$4.8^{+7.3}_{-3.1}$	$3.3^{+1.6}_{-0.8}$	53.5/50
5	15 04 09.7	−41 53 41	0.0015	$2.23^{+0.12}_{-0.13}$	$0.061^{+0.026}_{-0.026}$	22^{+15}_{-6}	$7.0^{+6.2}_{-5.0}$	$4.4^{+0.7}_{-0.9}$	73.3/67
	15 04 06.5	−41 51 25	0.0018	$2.21^{+0.10}_{-0.10}$	$0.050^{+0.023}_{-0.023}$	23^{+16}_{-6}	$8.4^{+7.5}_{-5.9}$	$6.2^{+1.5}_{-1.1}$	83.0/88
7	15 04 04.8	−41 49 35	0.0011	$2.19^{+0.11}_{-0.09}$	$0.038^{+0.027}_{-0.019}$	26^{+25}_{-13}	$9.3^{+21}_{-6.3}$	$8.7^{+8.8}_{-3.7}$	64.0/64
8	15 04 01.1	−41 49 22	0.0017	$2.20^{+0.09}_{-0.12}$	$0.044^{+0.022}_{-0.027}$	25^{+26}_{-9}	$7.3^{+12}_{-5.9}$	$6.2^{+5.1}_{-2.3}$	63.1/75
9	15 03 57.3	−41 48 08	0.0019	$2.20^{+0.07}_{-0.09}$	$0.045^{+0.023}_{-0.017}$	24^{+28}_{-6}	$7.7^{+9.5}_{-6.2}$	$5.8^{+3.9}_{-2.0}$	72.6/76
10	15 03 52.6	−41 46 58	0.0017	$2.20^{+0.07}_{-0.07}$	$0.045^{+0.020}_{-0.017}$	23^{+11}_{-5}	$8.5^{+6.7}_{-4.5}$	$6.3^{+2.8}_{-1.3}$	68.6/73
11	15 03 57.7	−41 45 28	0.00038	$2.20^{+0.07}_{-0.12}$	$0.058^{+0.028}_{-0.023}$	22^{+14}_{-4}	16.5^{+19}_{-10}	$11.1^{+7.9}_{-3.7}$	63.8/65
12	15 03 52.3	−41 43 31	0.00030	$2.21^{+0.07}_{-0.12}$	$0.057^{+0.031}_{-0.023}$	23^{+18}_{-10}	$13.5^{+26}_{-9.2}$	$9.5^{+13}_{-4.2}$	32.1/41
13	15 03 29.5	−41 42 03	0.0010	$2.24^{+0.11}_{-0.09}$	$0.069^{+0.030}_{-0.025}$	22^{+16}_{-8}	$5.5^{+10}_{-3.4}$	$3.7^{+2.6}_{-1.5}$	35.7/46
Mean	...	...	...	$2.22^{+0.08}_{-0.09}$	$0.051^{+0.007}_{-0.007}$	23^{+16}_{-17}	...	...	...

From left to right, the columns are the region number, right ascension and declination of the center of each extraction box, the fraction of the total 843 MHz MOST flux from the box, the differential spectral index, curvature parameter and exponential cut-off energy of the electron spectrum, the total magnetic field strength (not $B_\perp$), the cut-off frequency and goodness of fit. Uncertainties are reported at the 90% confidence level and include only the statistical contributions. These uncertainties were used as weights to compute the means. Note that the spectral indices and cut-off energies are not independent from region to region.

arithm of the momentum. If $a > 0$, then the spectrum flattens with increasing momentum. If $a < 0$, then the spectrum steepens with increasing energy. If $a = 0$, then the spectrum has no curvature and Eq. (1) reduces to the standard power law with an exponential cutoff.

For the set of spectral fits described here, $n_{\rm H}$ is fixed to be 6.0×10^{20} cm^{-2} (Allen, Petre & Gotthelf, 2001), the values of Γ, a and ϵ are same for the synchrotron and inverse-Compton models and the same synchrotron normalization is used for the X-ray and radio data. Except for $n_{\rm H}$, these parameters are free as is the inverse-Compton normalization and the total magnetic field strength (not $B_\perp$). The results of the fits for regions 1–13 are listed in Table 1 and the results for region 6, the region with the largest number of X-ray counts, are plotted in Fig. 2 to 4. In each case, the quality of the fit (χ^2/dof) is good.

3 Spectral index and curvature

The inclusion of spectral curvature as a free parameter systematically improves our measure of the goodness of fit. For example, the results for region 6 suggest that an uncurved electron spectrum (i.e., $a = 0$) can be excluded at about the 3.2σ confidence level. Similar results, with varying degrees of statistical confidence, are obtained for the other twelve regions. Collectively, the results provide a statistically compelling argument that the electron spectrum of SN1006 is curved.

While it may be argued that the improvement in the value of χ^2/DOF is due solely to the inclusion of an additional free parameter, there are two reasons to believe otherwise. First, the best-fit values of the spectral index and curvature are essentially the same from region to region (Table 1). If the improvement in the values of reduced chi-square was only due to the use of an additional free parameter, we expect that the range (0.038–0.079) and root-mean-square (0.012) of the distribution of best-fit curvature values would be larger. For example, some of the curvature values might be negative. Another reason is that the mean amount of curvature ($a = 0.051\pm0.007$), is consistent with the amount of curvature predicted for the proton (not electron) spectrum of SN1006. For example, Fig. 5 shows the best-fit electron spectra for region 6 in the two cases where the value of the curvature parameter

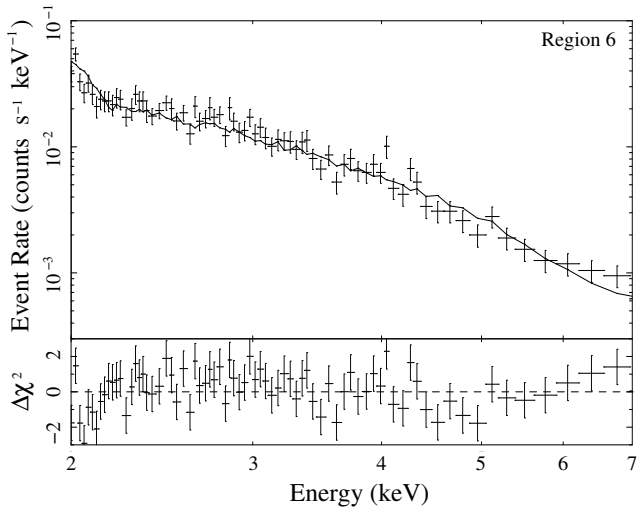

Figure 2: The ACIS spectrum for region 6. The top panel shows the sum of the source and background spectra (data points) and the sum of the best-fit model and background spectrum (solid line). The bottom panel shows the differences between the data points and the curve divided by the uncertainties in the data points.

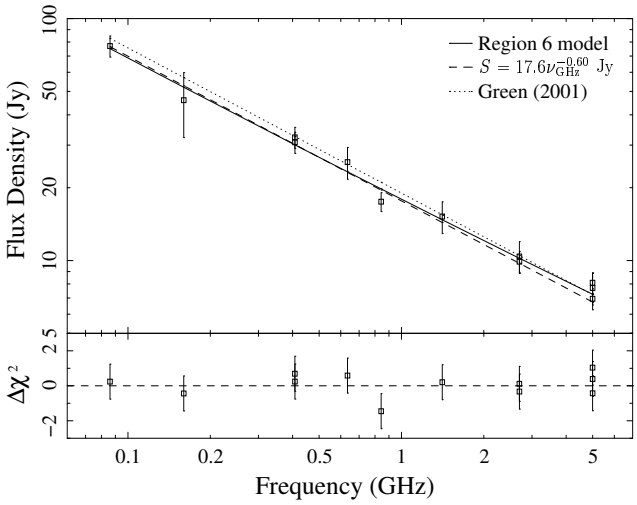

Figure 3: The radio spectrum for the entire supernova remnant. The top panel shows the source spectrum (data points) and three models. The dashed line is the best-fit power law $S(\nu) = 17.6^{+6.3}_{-4.8}(\nu/1\ \mathrm{GHz})^{-\alpha}$ Jy, where $\alpha = 0.60^{+0.08}_{-0.09}$. The dotted line is a power law using Green's (2001) spectral parameters ($S(\nu) = 19\ (\nu/1\ \mathrm{GHz})^{-0.6}$ Jy). The solid curve is the best-fit model for region 6 multiplied by the factor 0.00175^{-1} (see Table 1). The bottom panel shows the differences between the data points and the solid curve divided by the uncertainties in the data points.

is a free parameter and fixed at zero (solid and dashed curves, respectively). Neither spectrum is curved below $p = 1$ GeV/c, which was true during the fitting process, because the available data provide very little constraint on the shape of the electron spectrum in this momentum range. The top pair of dotted and dot-dashed curves are predictions described by Ellison, Berezhko & Baring (2000) for the proton (not electron) spectrum of SN1006. These spectra have been normalized to match the solid curve at $E = 0.9$ GeV. Since Ellison, Berezhko & Baring (2000) computed their spectrum assuming a spectral index of $\Gamma = 2.0$, instead of $\Gamma = 2.2$ (solid curve), it is not appropriate to compare the solid curve to the upper pair of dotted and dot-dashed curves. However, it is fair to compare the solid curve to the lower pair of dotted and dot-dashed curves because these two curves have been steepened to match the best-fit spectral index. Aside from a difference in the cut-off energy, the lower pair of theoretical curves match the solid curve remarkably well. The results of our fits suggest that the amount of curvature in the electron spectrum is the same as the predicted amount of curvature in the proton spectrum. For these reasons, we believe the improvement in the value of χ^2/DOF is not merely due to the inclusion of an additional free parameter.

Perhaps the greatest concern about the claim that the electron spectrum of SN1006 is curved is that one or more of the assumptions of the analysis are invalid. One assumption is that electron spectrum has the form of Eq. (1). This assumption seems to be vindicated by a comparison of the best-fit spectral shape for region 6 and predictions of the amount of curvature in the proton spectrum (Fig. 5). Another assumption is that the shape of the radio spectrum in each of the thirteen regions is the same as the shape of the radio spectrum of the entire remnant. If this assumption is invalid, the best-fit values of the spectral index and curvature may be inaccurate. Yet, the mean values of the index and curvature are robust. To assuage this concern would require good radio spectra for many, small, spatially-resolved features in the remnant. Unfortunately, this kind of data is not available for SN1006. Nevertheless, the similarities of the best-fit values of the spectral index and curvature from region to region and the similarity of the fitted and predicted curvature gives us some confidence that the electron spectrum of SN1006 is curved.

If spectral curvature is found to be a common feature of shell-type supernova remnants, then the results will emphasize the fact that cosmic rays are dynamically

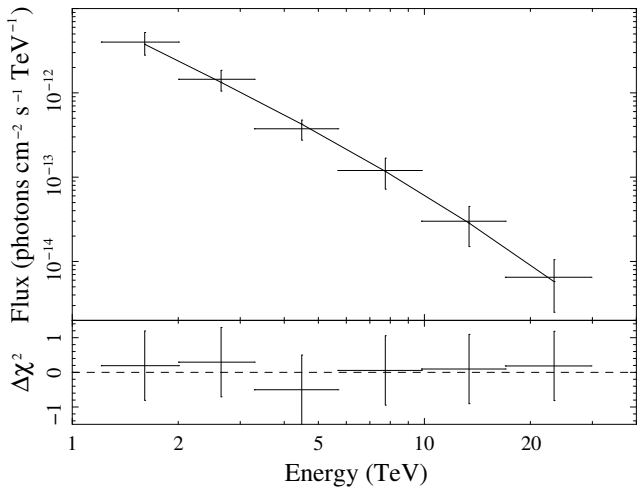

Figure 4: The CANGAROO spectrum for the entire eastern rim of SN1006 (Tanimori et al., 2001). The top panel shows the source spectrum (data points) and the best-fit model (curve). The bottom panel shows the differences between the data points and the curve divided by the uncertainties in the data points.

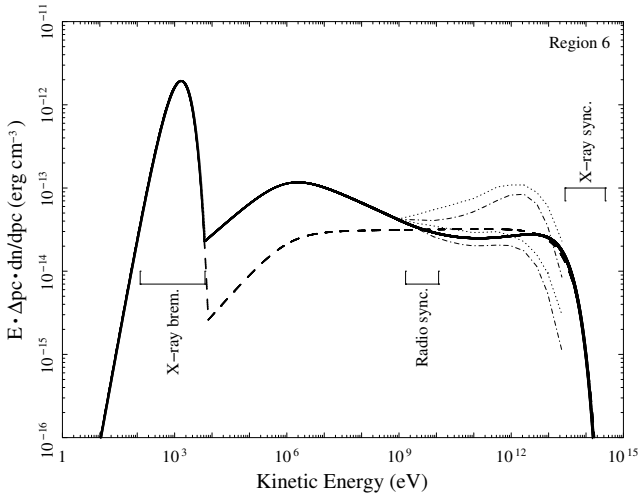

Figure 5: The best-fit electron number-density spectra for region 6. The solid and dashed curves are the spectra for the models with and without spectral curvature, respectively. The upper set of dotted and dot-dashed curves are the models for the proton (not electron) spectrum of SN1006 presented by Ellison, Berezhko & Baring (2000). These curves are plotted only for momenta $p > mc$ (i.e., the range of momenta to which our fits are sensitive) and are normalized to the solid curve at a kinetic energy of 0.9 GeV. As described in the text, the lower set of dotted and dot-dashed curves are the same pair of models multiplied by $(E/0.9\ \mathrm{GeV})^{-0.2}$. The amount of spectral curvature for our model of the electron spectrum is consistent with the amount of curvature reported by Ellison, Berezhko & Baring (2000) for the proton spectrum. From left to right, the three bracketed energy bands are primarily responsible for the observed thermal bremsstrahlung, radio synchrotron and X-ray synchrotron emission, respectively. The highest energy electrons also produce TeV γ-ray emission.

important. In this case, the evidence of spectral curvature may provide indirect evidence for the presence of cosmic-ray nuclei because the fraction of the internal energy ($\sim 10^{51}$ erg) in the form of non-thermal electrons ($\lesssim 10^{49}$ erg, Allen, Petre & Gotthelf, 2001; Dyer et al., 2001) may be too small to significantly affect the dynamics of the shock.

4 Cut-off energy and magnetic field strength

Aside from the electron spectral index and curvature, fits to X-ray and radio synchrotron data provide a measure of the frequency at which the synchrotron spectrum is cut off. This cut off in the photon spectrum is associated with a cut off in the electron spectrum (e.g., see Fig. 7 and 9 of Allen, Petre & Gotthelf (2001)). For relativistic electrons, the cut-off frequency

$$\nu_{\rm c} = 1.35 \times 10^{16} \left(\frac{\epsilon}{10\ \mathrm{TeV}}\right)^2 \left(\frac{B}{10\ \mu\mathrm{G}}\right)\ \mathrm{Hz}. \quad (2)$$

The results for the cut-off frequency are listed in Table 1. Since the cut-off frequency depends on the product $\epsilon^2 B$, it in not possible to uniquely determine the value of the cut-off energy using only the synchrotron data. Tanimori et al. (1998) report evidence of TeV γ-ray emission from SN1006. If this emission is produced by inverse-Compton scattering of the cosmic microwave background radiation, then the TeV data can be used to determine the cut-off energy of the electron spectrum. The values obtained for the cut-off energies and the magnetic fields strengths are listed in Table 1.

Since the same γ-ray data is used for each region, the best-fit cut-off energies for the thirteen regions are consistent with the mean cut-off energy. However, the actual cut-off energy may vary from region to region. A constant value for the cut-off frequency (i.e., $5.02^{+0.44}_{-0.45} \times 10^{16}$ Hz, 90% confidence level) can be excluded at the 2.9σ confidence level. Since the cut-off frequency $\nu_{\rm c} \propto \epsilon^2 B$, a variation in the cut-off frequency requires a variation in either the cut-off energy or the magnetic field strength. It is not possible to determine whether the apparent variation in the cut-off frequency is due to a variation in the magnetic field strength or the cut-off energy. However, it is interest-

ing that the location of the peak of the TeV emission (the triangle in Fig. 1) is near the two regions with the largest cut-off frequencies. Although this result is not statistically compelling, it suggests that the cut-off energy may be larger in this region. Likewise, if the cut-off frequency of the southwestern rim is found to be smaller than the cut-off frequency of the northeastern rim, then the lack of observed TeV emission from the southwest may be due to a reduced cut-off energy in the southwest.

As a final caveat, it should be noted that if the TeV γ-ray emission is not produced by inverse-Compton scattering of the cosmic microwave background radiation or if the the results of Tanimori et al. (1998) are inaccurate, then the results for the cut-off energies and magnetic fields are meaningless. Yet, the results for the spectral index, curvature and cut-off frequency remain valid within the constraints of the assumptions described in Sect. 3. The discovery of evidence of a curved cosmic-ray electron spectrum is robust.

5 Conclusions

For the first time, we simultaneously fitted X-ray, radio and γ-ray spectral data for the the northeastern rim of SN1006. The X-ray and radio data were fitted with a synchrotron emission model. The γ-ray data were fitted with a model of inverse-Compton scattering of the cosmic microwave background radiation. The photon spectra for both models are based on an electron spectrum that has a momentum-dependent power-law index. The rate of change in the index for each decade in momentum is a free parameter of the fit. If our assumptions are valid, then the results clearly show that the GeV to TeV electron spectrum is curved. The best-fit power-law index at 1 GeV (i.e., radio–synchrotron-emitting energies) is $2.22^{+0.08}_{-0.09}$. At 30 TeV, the electron spectrum has flattened to have an effective index of 1.99 ± 0.09 (90% confidence level uncertainties). This amount of curvature is quantitatively consistent with predictions of the amount of curvature in the proton spectrum of SN1006.

The existence of a curved cosmic-ray spectrum suggests that cosmic rays are not "test" particles. The pressure of the cosmic rays is large enough to modify the shock structure. Since non-thermal electrons contain only about 1% or less (i.e., $\lesssim 10^{49}$ erg) of the total internal energy, the presence of curvature may provide indirect evidence of a much more energetic population of cosmic-ray protons. If remnants other than SN1006 and Cas A (Jones et al., 2003) are found to exhibit evidence of a curved synchrotron spectrum, then the results will help demonstrate that efficient particle acceleration is a common feature of supernova remnants.

Acknowledgments

This work grew out of discussions with Don Ellison regarding the shape of cosmic-ray spectra. Chuck Dermer's encouragement lead to the development of synchrotron and inverse-Compton models for curved electron spectra. This work benefited substantially from discussions with Tom Jones and Steve Reynolds. We thank John Davis for his helpful suggestions concerning some of the details of the computation of the synchrotron flux.

References

Allen, G. E., Petre, R., Gotthelf, E. V. 2001, ApJ, 558, 739

Dyer, K. K., Reynolds, S. P., Borkowski, K. J., Allen, G. E., Petre, R. 2001, ApJ, in press

Ellison, D. C., Berezhko, E. G., Baring, M. G. 2000, ApJ, 540, 292

Green D. A. 2001, "A Catalogue of Galactic Supernova Remnants (2001 December version)", available at http://www.mrao.cam.ac.uk/surveys/snrs/

Houck, J. C., Denicola, L. A., 2000, in ASP Conf. Ser. 216: Astronomical Data Analysis Software and Systems IX, 591

Jones, T. J., Rudnick, L., DeLaney, T., Bowden, J. 2003, ApJ, 587, 227

Lagage, P. O., Cesarsky, C. J. 1983, A&A, 125, 249

Reedy, R. C., Arnold, J. R., Lal, D. 1983, Annu. Rev. Nucl. Part. Sci., 33, 505

Roger, R. S., Milne, D. K., Kesteven, M. J., Wellington, K. J., Haynes, R. F. 1988, ApJ, 332, 940

Tanimori, T., et al. 1998, ApJ, 497, L25

Tanimori, T., et al. 2001, in Proc. 27th Int. Cosmic Ray Conf. (Hamburg), 6, 2465

Winkler, P. F., Long, K. S. 1997, ApJ, 491, 829